Cellulose manuscript No.
(will be inserted by the editor)

Estimating the transverse dimensions of cellulose fibres in wood and paper using 2D and 3D microscopy techniques

N. J. McIntosh · Y. Sharma · D.M. Martinez · J.A. Olson · A.B. Phillion

Received: 29 August 2018 / Accepted: 22 December 2018

Abstract We describe a duo of experimental methods for determining the transverse dimensions of individual wood fibres using 2D optical microscopy and 3D x-ray tomography. These non-invasive optical sectioning methods, in conjunction with segmentation through image analysis, enables *in situ* identification of individual fibres in a paper sheet. The relationship between local fibre dimensions, *i.e.* diameter and fibre wall thickness are established for kraft (NBSK) pulp fibres and compared to values obtained from wood. For the first time, we propose a criterion for transverse fibre collapse during the papermaking process that is based on both fibre diameter and wall thickness.

Keywords softwood fibres · paper physics · characterization · 2D optical microscopy · 3D X-ray tomography · Delaunay triangulation · lumen tracking

1 Introduction

Refiners are machines comprised of two, parallel, counter-rotating, grooved metal plates; material (wood chips or pulp) is fed into the center of one of the plates and flows radially outward between the plates, being abraded as it does so. The case of wood chips being fed into the refiner is known as high consistency (HC) refining or simply pulping, while the case of pulp being fed into the refiner is known as low consistency (LC) refining. Generally speaking, HC refining serves

N.J. McIntosh · D.M. Martinez

Department of Chemical and Biological Engineering, The University of British Columbia, Canada E-mail: mark.martinez@ubc.ca

Y. Sharma · J.A. Olson

Department of Mechanical Engineering, The University of British Columbia, Canada

A.B. Phillion

Department of Materials Science and Engineering, McMaster University, Canada E-mail: philliab@mcmaster.ca

to dismantle wood chips into their constituent fibres, while LC refining serves to develop the properties of the fibres such that they are better suited to the desired fibre product properties.

During LC refining the physical morphology of the cellulose fibre is modified by applying a repetitive force. Early researchers recognized that there were a number of different effects (Horn, 1978); these were then classified into two categories: cutting or splitting of the fibre, and, fibrillation of the internal or external surfaces. Internal fibrillation, the loosening of the cell wall structure, aids in swelling and fibre flexibility. External fibrillation is restricted solely to the outer surface and is characterized by the loosening of the cellulose fibrils. Today, it is recognized that there are numerous beating effects in addition to the ones described above.

The morphological properties of pulp fibres, particularly their transverse dimensions (*i.e.*, wall cross-sectional area, perimeter, and thickness) strongly affect the properties of the paper sheet (Schulgasser and Page, 1988; Johansson, 2011; Seth, 1990). Traditionally, these properties were determined through mechanical sectioning followed by optical microscope image evaluation (Hirn and Bauer, 2006). However, this methodology is tedious and prone to artifacts as fibre orientation is non-isotropic. More recently, sophisticated techniques involving scanning-electron microscopy (SEM) (Reme et al., 2002), confocal laser scanning microscopy (CLSM) (Jang et al., 1992, 2005), and X-ray tomographic microscopy (μCT) (du Roscoat et al., 2007; Sharma et al., 2015), among others, have been developed and coupled with advanced image analysis (Xu and Ting, 1996). The choice of the imaging modality depends on the desired resolution and field of view, and the properties under study. To give an example, while CLSM and μCT provide images at the sub-micron resolution, SEM emable visualization of nano-scale features (Chinga-Carrasco, 2009).

The present study is motivated by a need to better understand the changing the transverse dimensions of individual fibres inside a fibre mat resulting from release of the wood matrix and subsequent processing. For wood fibres, optical microscopy is a proven successful technique given the propensity for the fibres to all grow in the vertical direction. For paper fibres, however, the refining process results in a complex 3D fibre mat structure. In this case, μCT is a valuable technique for revealing the 3D tortuous and inter-connected morphology of paper architecture. In this work, high-quality 2D cross-sectional optical images of wood samples (softwood) made by mechanical sectioning are compared to high quality 3D X-ray tomographic images of paper samples. All of the images are then analyzed for individual fibre transverse dimensions - cross-sectional area, perimeter, and wall thickness. The work is focused on slow growing softwood i.e. spruce, pine and fir having low coarseness fibres which are susceptible to fibre wall collapse.

2 Methods

2.1 Two-dimensional Imaging of Wood

Transverse sections of wood chips 30μm thick were imaged at 10× magnification using a top-mounted digital camera on a Nikon light transmission stereo microscope. These samples were prepared using a sledge microtome and subsequently dyed blue and mounted on glass microscope slides using Permount mounting medium (Fisher Chemical). Figure 1a gives an example of the type of raw images collected using this method.

Before fibre dimensional statistics (*i.e.*, fibre diameter, wall thickness) were able to be gleaned from the images, a preprocessing step was completed. Specifically, the images were binarized using an Otsu binarization procedure (Otsu, 1979) to determine the voidspace (lumens) and solid (fibre walls), and then analyzed to collect the set of contours that represent the fibre wall / lumen boundaries. The correspond regions Ω_l enclosed by each contour l identify individual lumens. To calculate the area of each Ω_l, and coordinates of its centroid, $\mathscr{C}_l$, the corresponding moments M_l^{ij} were calculated as:

$$M_l^{ij} = \sum_{\Omega_l} x^i y^j \mathscr{P}_{xy} \mathrm{d}A, \tag{1}$$

where $\mathscr{P}_{xy}$ is the pixel value at point (x,y) in the image. Due to the binarization step, the value of a pixel in the image is either 0 or 1 and is 1 for all pixels within each Ω_l. The x and y coordinates of the centroid $\mathscr{C}_l$ of each lumen's voidspace are then given by M_l^{10}/M_l^{00} and M_l^{01}/M_l^{00}, respectively, while the area of each lumen A_l is simply M_l^{00}.

Calculation of the lumen circular equivalent diameter D^l is straightforward given a value of lumen area:

$$D_l = \left(\frac{4A_l}{\pi}\right)^{(1/2)}. \tag{2}$$

The calculation of the outer fibre diameter and wall thickness required the development of a method based on a Delaunay triangulation. To set up the triangulation, the centroids of each of the lumens found according to the above method were used as the vertex points in the triangulation. Once the triangulation was computed the average wall thickness of two adjacent (*i.e.*, connected by a triangle edge) fibres as well as outer diameters could be calculated. For each edge in the triangulation, the centroid-to-centroid distance L was given, simply, by the magnitude of the difference vector between centroids:

$$L_{l+1,l} = ||\mathscr{C}_{l+1} - \mathscr{C}_l||. \tag{3}$$

Since the area of each lumen under consideration is known from the binarization/contour finding procedure already completed, the circular-equivalent radius may be straightforwardly calculated as

$$R_l = \sqrt{\frac{A_l}{\pi}}. \tag{4}$$

The average wall thickness between two, edge-connected fibres is then given by:

$$w_{l+1,l} = \frac{L_{l+1-l} - R_{l+1} - R_l}{2}. \tag{5}$$

An estimate of the outer diameter of each fibre can then be calculated as the sum of the lumen's circular-equivalent radius and the wall thickness: $D = 2(R + w)$.

The above procedure may be applied to an arbitrary number of images to obtain an arbitrary number of fibre measurements and corresponding diameter/wall thickness distributions. Ensuring that the sampled images were representative of the wood matrix under consideration was accomplished by monitoring the convergence of the fibre diameter distribution. More specifically, a Gaussian mixture model was fit to progressively larger samples (*i.e.*, more images worth of data) until the model parameters converged to a single value. A distribution was marked as 'converged' when, upon introduction of additional data, the model parameters changed by less than 1% relative to the previous values without the additional data. The Gaussian mixture models used in this work were defined to be a weighted sum of K Gaussian distributions ($\mathcal{N}$):

$$f(D) = \sum_{k=1}^{K} w_k \mathcal{N}(D|\mu_k, \sigma_k^2). \tag{6}$$

In the above, w_k are the component weights that satisfy:

$$\sum_{k=1}^{K} w_k = 1, \tag{7}$$

where μ_k is the kth component's mean, and σ_k^2 is the kth component's variance. From a practical point of view, the diameter distribution was found to converge when approximately 10 000 fibres were sampled; the dataset presented in this work (c.f., Figure 3) contains 11909 fibre measurements.

2.2 Three-dimensional Imaging of Paper

The method presented in the previous section only provides a two dimensional image of the specimen. X-ray micro computed tomography is a three dimensional non-destructive imaging technique which provides high resolution images

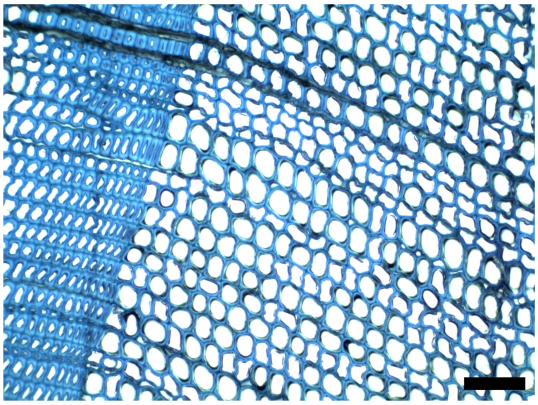

(a)

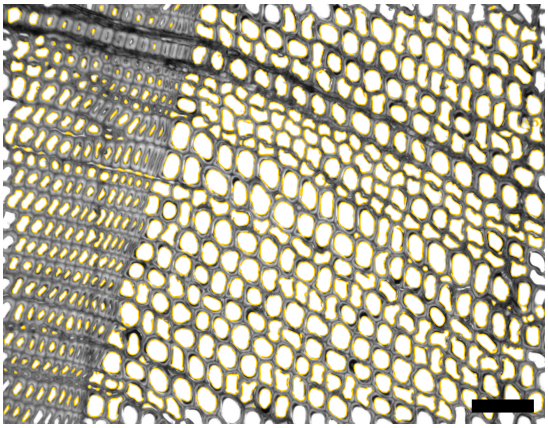

(b)

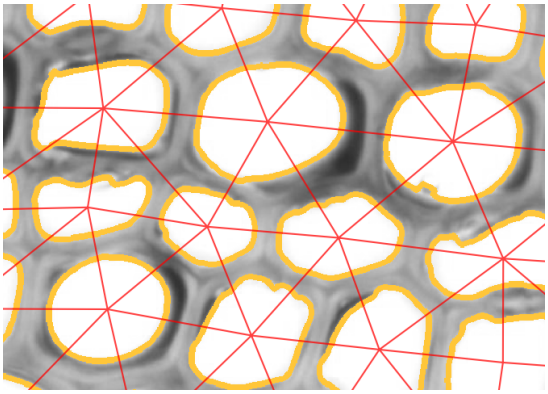

(c)

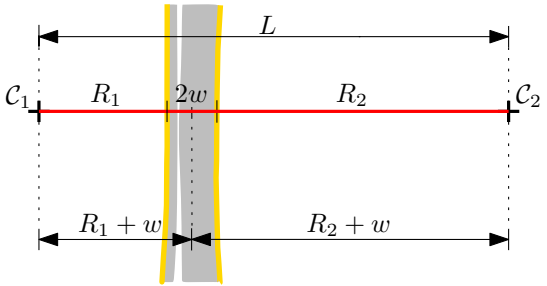

(d)

Fig. 1: Images of: optical microscope image of sectioned, dyed wood used for image analysis and fibre data extraction (Figure 1a), voidspace contours overlaid on original image (Figure 1b), detail view of the Delaunay triangulation drawn on a portion of a microscope image (Figure 1c), and geometrical setup of Delaunay triangulation for wall thickness and diameter computation (Figure 1d). Note that the scale bars in the images are 100µm in length.

of the internal structure of materials making it a very useful tool for material science (Withers, 2007). However, μCT imaging of paper poses several challenges owing to the low attenuation coefficient of wood fibres. Past research, summarized in the review by Bloch (J.-F. Bloch, 2009), has found success in segmenting fibres using the lumen as markers because they are separated from the background by means of thick fibre walls. Due to the large number of fibres, the segmentation method must also be automated. A number of researchers have attempted to automate the segmentation by automatically identifying lumen cross-sections (Aronsson, 2002; Kontscheider et al., 2010; Bache-Wiig and Henden, 2005). Donoser et al. (Donoser and Bischof, 2006) developed an efficient algorithm to track lumen in 3D by simultaneously detecting and tracking the lumen cross-sections as maximally stable external regions (Matas et al., 2004). Kontscheider et al. (Kontscheider et al., 2010) demonstrated the successful identification of lumen in 2D microtomy images using a novel shape descriptor (Donoser et al., 2009; Lu et al., 2009). Aronsson (Aronsson, 2002) automated and improved the process by first detecting lumen cross-sections and then applying constraints on area and curvature. Bache-Wiig et al. (Bache-Wiig and Henden, 2005) extended this idea by adding additional physical constrains (bending energy, eccentricity, and convexity). Recently, Sharma (Sharma et al., 2015) proposed a three-step segmentation algorithm that was able to link un-collapsed fibres with their corresponding collapsed sections. This method was then benchmarked using a series of known test specimens produced from thin-walled aluminum tubes (Sharma et al., 2015).

Sharma et al. (Sharma et al., 2015) presented a method to image small sections of paper handsheets at a voxel size of 0.58 μm. Figure 2a shows a 3D image of a paper handsheet manufactured using 100% never-dried NBSK pulp and imaged using a Zeiss Versa XRM 400 x-ray tomographic microscope. The NBSK was Low Consistency refined in an 12” Aikawa refiner, details given in (Mithrush, 2013) using a fine bar plates at 3% consistency. The refiner was operated in re-circulation mode with at a fixed specific energy, created by adjusting the gap between the plates. The handsheet making was performed using TAPPI standard T205. The handsheet was not mechanically pressed but instead directly freeze dried, in restraint. The use of freeze drying minimizes morphology changes resulting from capillary effects.

Figure 2b shows 4 unique fibres segmented from the image in Figure 2a using the fibre segmentation algorithm presented by Sharma et al. (Sharma et al., 2015). The algorithm uses fibre lumens in 2D slices to initiate a fibre trace based on connectivity along the longitudinal direction. Since the method uses lumens as the markers for fibre segmentation, it is unable to segment completely collapsed fibres, however, it can segment partially collapsed fibres *i.e.* the fibres which have a lumen in certain sections with intermediate collapsed sections. The algorithm assigns a unique label to the lumen and fibre wall belonging to each segmented fibre. As can be seen in Figure 2b, the topology of the segmented fibres is preserved when using this fibre segmentation algorithm. Altogether, approximately 1000 fibres were identified in Figure 2a.

Using the segmented 3D volume shown in Figure 2a, fibre statistics (diameter and wall thickness) can be obtained. Given that it is a 3D dataset, these quantities are not unique values for each fibre, but actually vary along the fibre length. Analyzing the dataset is equivalent to sectioning each fibre into 0.58µm thick slices. For every slice, the diameter of an equivalent circle that has the same area as the fibre+lumen cross-section in that slice can be computed. The equivalent outside diameter D is thus:

$$D_\ell = 2\sqrt{A_\ell/\pi}, \tag{8}$$

where ℓ represents each identified fibre+lumen cross-section in the 3D dataset, and A_ℓ is the calculated area of the fibre+lumen cross-section. Similarly, the lumen area A'_ℓ by counting the number of pixels inside the lumen of each. The wall thickness w_ℓ is then given by:

$$w_\ell = \sqrt{A_\ell/\pi} - \sqrt{A'_\ell/\pi}. \tag{9}$$

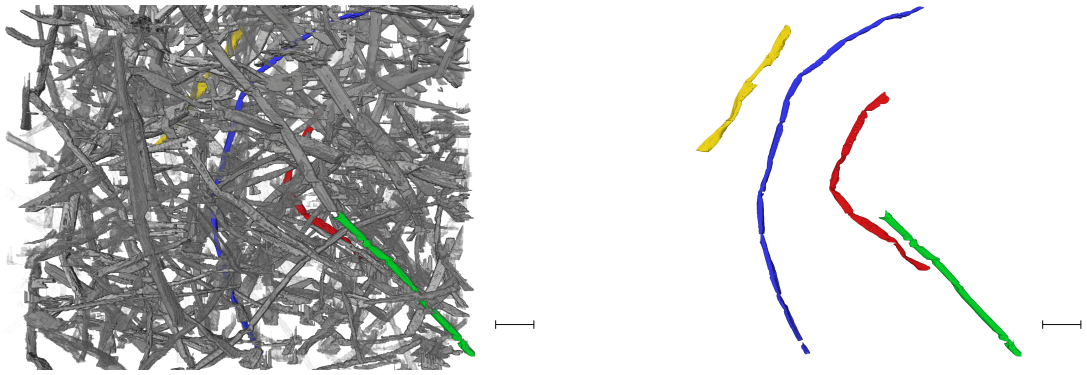

(a) (b)

Fig. 2: Figure 2a shows the 3D matrix of fibres imaged using x-ray µCT imaging with selected fibres colored. Figure 2b shows the same imaging volume with all but selected fibres removed to show full 3-dimensional structure. Note that the scale bars in the images are 100µm in length.

3 Results and Discussion

The source fibres considered in this study are a mixture of softwood species (in both the two- and three-dimensional imaging). Normalized frequency (denoted f) distributions of the fibre diameters and wall thicknesses obtained using the methodologies outlined above are given in Figure 3.

Considering first the wood dataset, the skewness owing to the earlywood/latewood variation within the fibre population can be seen. The high number of large diameter, thin-walled earlywood fibres relative to the few small diameter, thick-walled latewood fibres is evident in the positively skewed diameter and negatively skewed wall-thickness distributions. Second, assuming that the difference between the wood and paper datasets is due to the combined effects of all the pulping/papermaking processes the fibres have undergone, it is possible to assess the effectiveness of processing on the changes to the fibre morphology. In both the diameter and wall thickness cases, two similar effects are observed: a shift in the distribution towards smaller values, and a distribution-narrowing/homogenization effect.

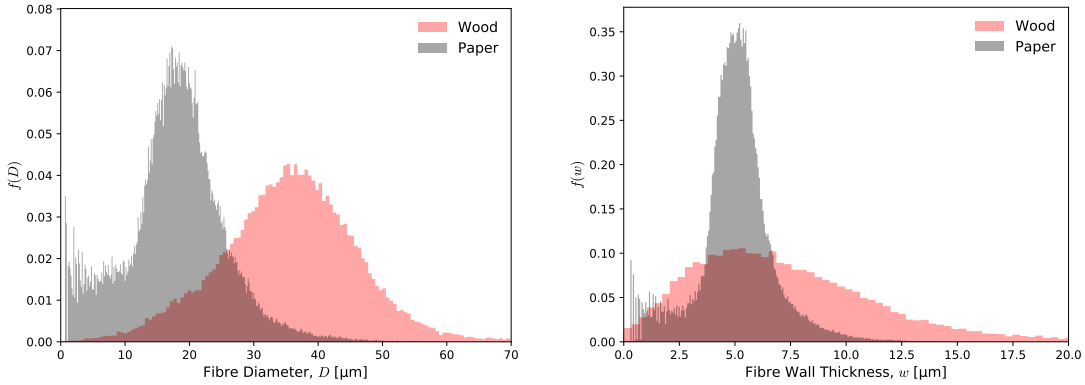

Fig. 3: Histogram of fibre diameters and wall thicknesses sampled from both wood and paper using the optical and x-ray tomogaph methods.

Noticeable in both the wall thickness and diameter distributions is a peak in frequency of small values measured, *i.e.*, there is a much higher rate of incidence of very small diameter, very thin-walled fibres in the paper samples measured using the µCT method when compared to those fibres in the wood samples measured using optical microscopy. This behavior in the distributions can be explained by considering a combination of two related effects having to do with the two unique imaging methods used for wood and paper samples. First, the apparent scarcity of small, thin-walled fibres in the wood matrix owes to the fact that the triangulation method determines the combined wall thickness of two adjacent fibres, which are assumed to be equal and not individual fibre walls. In regions of sharp gradients from early wood to late wood this will create artifacts.Second, all fibres regardless of their absolute dimensions or location along the fibre axis are identified in the µCT data because of the manner in which the segmentation algorithm was developed. Thus, it is thought that the peak at the lower end of the diameter and wall thickness distributions for fibres in paper is due to the fact that small fibres and the slender fibre ends are simply not measured in the two-dimensional wood case, while in the three-dimensional µCT case they are. It must be noted that the wall thickness estimates found for the paper, at approx. 5 µm, are significantly larger than those found previously. A commonly-reported value for NBSK is approx. 3 µm (Watson

and Bradley, 2009). It is hypothesized that this is a result of sampling bias in the 3D fibre tracking algorithm; only the fibres that survive the LC refining process intact, containing lumen, are reported. Thus, the distribution shown in Figure 3 is not representative of the true cell wall distribution but a larger value due to sampling bias.

Another quantity often of interest when assessing the physical properties of fibres is the coarseness. Traditionally, coarseness is a measure of the linear mass density of a fibre and has dimensions of mass per unit fibre length. Since in this work the only measurements gathered were the fibre dimensions, a rough area-based analog of coarseness, A, was defined and used in later analysis. For a pair of fibre dimensions D and w the 'area coarseness' was defined as:

$$A \triangleq \log\left[\frac{w^2 - Dw}{\mu_D^2}\right] \tag{10}$$

where μ_D is the average fibre diameter considering all measurements taken. It is instructive to note that the logarithm and denominator in the above definition of A serve no physical purpose, instead they are used simply as a convenient scaling method to make the values of A more tractable. Using Equation 10 and the data presented in Figures 3, a frequency distribution of A values for the fibres measured was created and is shown in Figure 4. As can be seen, the fibres in paper are less coarse than those in wood.

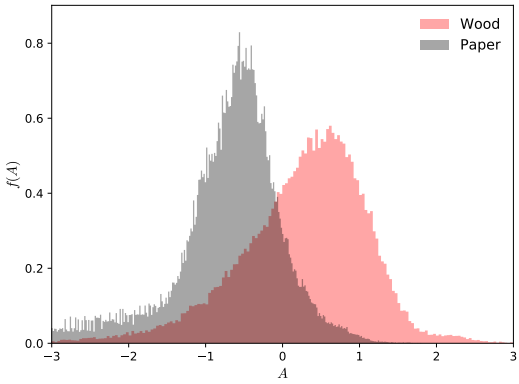

Fig. 4: Fibre area coarsenesses calculated using the fibre diameter and wall thickness data sampled from wood and paper using the optical and x-ray tomograph methods.

The ability of the μCT method to accurately measure the diameter of the slender tips of the fibres embedded in the paper matrix can be seen in Figure 5 where a series of diameter measurements (scaled by the average wall thickness of the given fibre μ_w) from two-dimensional slices determined to be from a common fibre are plotted along the axial length of the fibre. Of particular interest in this plot are two features: that the diameter of the narrowing ends of the fibres are resolved until the diameter effectively reduces to zero and the presence of apparent fibre collapse occurring at roughly 30

μm and 250 μm along the length of the fibre. Scaling the calculated fibre diameter by the average wall thickness μ_w of that fibre allows for the comparison of the diameter to the theoretical minimum for a fully collapsed fibre where $D = 2w$.

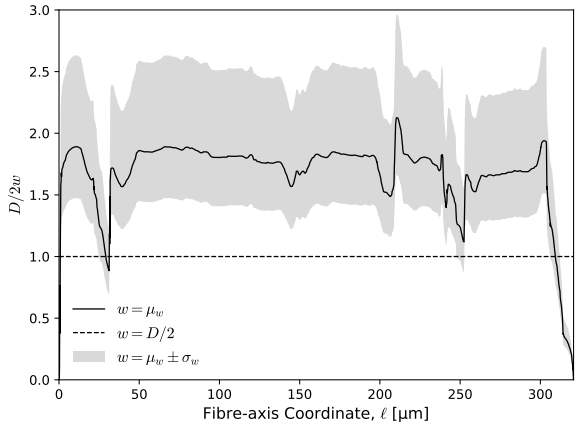

Fig. 5: Plot of fibre diameter (normalized by fibre wall thickness) for a single fibre from μCT data for a single fibre in a paper matrix along its axis, ℓ. Note the total collapse that occurs at roughly 30 and 250 μm along the fibre axis. Plotted is the fibre diameter normalized by mean wall thickness μ_w and one wall thickness standard deviation σ_w above and below the mean.

The same measurement points in Figure 5 that show the collapse of the fibre can be seen (along with similar measurements from other fibres) on the $w = D/2$ line on the main plot in Figure 6. The main plot in this figure is the entire collection of measurements taken from both wood and paper samples plotted in $D - w$ space. Analyzing this plot reveals four main features unique to the paper fibre measurements:

- Measurements of full fibre collapse lying on the $w = D/2$ line.
- A relative scarcity of partially collapsed/thick-walled fibres, along with a gap between fully collapsed fibers on the $w = D/2$ line and the bulk of the other measurements.
- A relative scarcity of thin-walled fibres, suggesting that that fewer of them were found in the 3D volume.
- A relative scarcity of large diameter fibers as compared to the wood.

Each of the above features warrants discussion. First, the presence fibers along the $w = D/2$ line identifies that fibre collapse is present, at least in some form, in the finished paper product. However, the homogeneity of the fibre collapse can be called into question. This is because the fibre segmentation algorithm tracks the void (*i.e.*, lumen) space inside of the fibres between adjacent 3D slices and decides which 2D features (*i.e.*, fibre cross sections) belong to a common fibre based on continuity. Thus, solid fibres are not be detected because no continuous lumens can be tracked. The design of

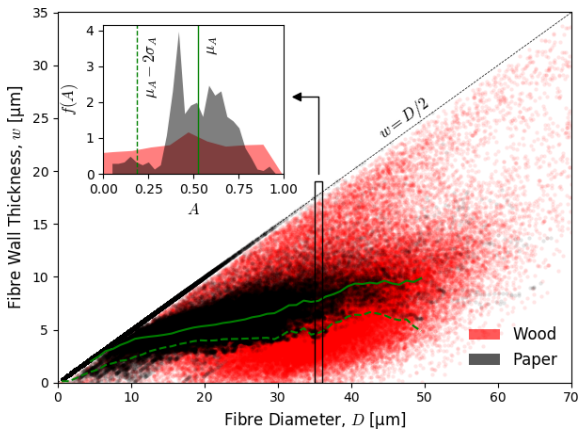

Fig. 6: Fibre wall thickness vs. fibre diameter for sample data from both wood and paper. The inset plot illustrates how the empirical threshold for collapse was found: two standard deviations below the mean of the distribution of area coarseness values translates well to the threshold observed in the data in $D - w$ space. Fibres with a wall thickness thinner than the threshold are believed to be those which collapse.

the algorithm, then, suggests that the fully collapsed measurements seen in Figure 6 (those which lie on the $w = D/2$ line) are distributed over the length of different fibres. This indeed seems to be the case when a single fibre's dimensions are considered, as in Figure 5. Since the wall thickness is variable over the length of the fibre, whether or not μ_w is the appropriate scaling factor for the diameter can be questioned. Accordingly, upper and lower bounds on the scaling are given by considering a wall thickness one standard deviation above and below the mean wall thickness $\mu_w \pm \sigma_w$. Even when considering this modified scaling, full fibre collapse is observed to occur at the same locations as are observed with a scaling only by μ_w.

Second, the lumen tracking mechanism also explains the lack of measurements of partially collapsed/thick-walled fibres. In either the case of a fibre having a very thick wall or one that is very uniformly nearly collapsed (those fibres lying just under the $w = D/2$ line), the accurate and consistent tracking of a lumen between image slices becomes difficult and can potentially fail. This measurement difficulty leads to the observed lack of thick-walled or uniformly partially collapsed fibres. The observed gap in the data just under the $w = D/2$ line, then, is presumably due to the combined effects of the lumen tracking algorithm systematically failing with these difficult to reconstruct fibres and the decoarsening (as well as distribution narrowing) effects seen in the plots in Figures 3.

Third, what is interesting is the apparent lack of thin-walled fibers in the paper samples when compared to those in wood. It is suggested that the thinnest walled fibres are the ones that fully collapse and thus move from the bottom of Figure 6 to the line $w = D/2$ as a result of pulping/papermaking. Evidently, it seems, that a threshold exists for this

fibre collapse to occur. In the inset plot of Figure 6, the frequency distribution of the area coarseness of the fibres having diameters of 35-36 μm (those in the black box in the main plot) is shown. Taken at a (roughly) constant diameter, the values of area coarseness for the fibres can be interpreted as an analog for the wall thickness or, more physically, the fibre bending stiffness. Marked on the inset plot is the mean μ_A (solid vertical line) of the coarseness distribution as well as the point two standard deviations below the mean $\mu_A - 2\sigma_A$ (dashed vertical line). The coarseness values two standard deviations below the mean are observed to decently well describe the boundary between the collapsed and uncollapsed fibre regions. To see this more clearly, the coarseness thresholds found at a constant diameter over the measurement range (1μm steps were taken) were mapped back to w values. These mapped values are plotted as solid and dashed lines in the main plot of Figure 6. As can be seen, this choice of threshold seems adequately describe the threshold below which the thin-walled, less coarse fibres are though to collapse. As this threshold was found purely empirically, it is not expected that this rule would describe a broader set of measurements as a more phenomenologically-found threshold would. Rather, it is used here as a straightforward way to illustrate the existence of a threshold. Fourth, the lack of large diameter fibres present in the paper measurement set owe to, presumably, the combined effects of refining and fractionation in the pulping/papermaking process.

Based on the observations made in Figure 6, it is clear that the occurrences of fibre collapse are not distributed uniformly along the length of a fibre. Rather, ‘pinch points‘ along the length of a single fibre exist and speak to the fibre-level inhomogeneity of the pulping process. The existence of these pinch points along the fibre axis is a result of the refining process. It is postulated that the inhomogeneous mechanical treatment of fibres during LC refining causes the pinch points that are seen in our measurements. As pulp flows into an LC refiner it travels through the grooves in the plates. Occasionally a group of fibres will be caught between high points on the plates resulting in fibre compression/shearing (Mithrush, 2013). It is this cyclic force application that mechanically alters the fibre properties. Considering the variable nature of the native fibre properties combined with the non-isotropic nature of the fibre groups caught between refiner plates it is very likely that during compression/shearing, the forces along a fibre will be non-uniform. Specifically, forces will be higher on a section of fibre that crosses over an adjacent one, and a so-called ‘pinch point‘ will be created. Other scenarios could also exist that that result in non-uniform fibre loading during LC refining; in all cases this would result in the development of ‘pinch point‘,*i.e.*, non-uniform fibre collapse.

4 Conclusions

A duo of novel experimental methods have been employed to measure the dimensions of wood fibres both in their native wood matrix and in the finished paper sheet. A method which depends upon the construction of a Delaunay triangulation

from 2D optical microscope images of wood has been shown to be able to access the transverse dimensions of fibres while a 3D X-ray micro tomograph technique, in conjunction with a developed lumen tracking algorithm, has been used to access fibre dimensions from fibres still embedded in a finished paper sheet. Although successful in measuring full fibre collapse and general fibre structure, both methods possess measurement bias. The 2D imaging fails to detect very small fibres at all while the 3D imaging technique systematically excludes very thick-walled or very uniformly collapsed fibres by way of the lumen tracking algorithm breaking down. Even with the method's shortcoming considered the data was able to be examined quantitatively. However, more work is needed to extend the methodology to other pulps and processing methodologies.

Based on the data collected with the developed methods, the effects of pulping/papermaking on the dimensions of softwood fibres was directly assessed. Homogenization with respect to the distributions of both the fibre diameter and wall thickness was observed; the distribution of an 'area coarseness' quantity computed from the measured values of diameter and wall thickness was also observed to narrow somewhat moving from fibres in wood to those in the finished paper product. The mean value for each of these dimensions was also observed to be reduced, presumably from the abrasive and size selective steps in the pulping and papermaking processes. Following from the reduction of the fibre dimensions through pulping/papermaking, fibre collapse was observed in the measured set of fibres in paper. However, the fibre collapse was not uniform along a fibre, but rather occurring inhomogeneously at 'pinch points'. The existence of these pinch points can be explained by considering the geometry and operation of the LC refining process. Finally, an empirically-found threshold was presented which, at least for the given set of measurements, well describes the cut-off for full fibre collapse. Treating the area coarseness quantity defined in Equation 10 as an analog for fibre bending stiffness, a lower bound of wall thickness required to avoid collapse was found which corresponds to two standard deviations below the mean fibre area coarseness. A more physically based method for determining the threshold likely exists but the presence of such a threshold is nonetheless clear.

5 Acknowledgements

The authors thank Canfor Pulp Products Inc. and the Natural Sciences and Engineering Research Council of Canada (NSERC) for funding this work. A large portion of the optical microscopy work was completed as part of the Energy Reduction in Mechanical Pulping research program at The University of British Columbia, all of the program partners are thanked for their support.

References

M. Aronsson. *On 3D fibre measurements of digitized paper*. Phd thesis, Swedish University of Agricultural Sciences, 2002.

J. Bache-Wiig and P. Henden. Individual fiber segmentation of three dimensional microtomograms of paper and fiber-reinforced composite materials. Masters thesis, Norwegian University of Science and Technology, 2005.

G. Chinga-Carrasco. Exploring the multi-scale structure of printing paper - a review of modern technology. *Journal of Microscopy*, 234:211–242, 2009.

M. Donoser and H. Bischof. Efficient maximally stable extremal region (mser) tracking. *IEEE Computer Society Conference on Computer Vision and Pattern Recognition*, pages 553–560, 2006.

M. Donoser, H. Riemenschneider, and H. Bischof. Efficient partial shape matching of outer contours. *Lecture Notes in Computer Science*, 5994:281–292, 2009.

S. R. du Roscoat, M. Decain, X. Thibault, C. Geindreau, and J.-F. Bloch. Estimation of microstructural properties from synchrotron x-ray microtomography and determination of the rev size in paper materials. *Åcta Materialia*, 55: 2841–2850, 2007.

U. Hirn and W. Bauer. A review of image analysis based methods to evaluate fiber properties. *Lenzinger Berichte*, 86: 96–105, 2006.

R. A. Horn. Morphology of pulp fiber from hardwoods and influence on paper strength. resreport, Forest Products Laboratory, Forest Service, United States Department of Agriculture, Madison, Wisconsin, 1978.

S. R. d. R. J.-F. Bloch. review: 3d analysis of paper. *FRC 2009, 14th Fundamental Research Symposium, Advances in Pulp and Paper Research*, pages 599–664, 2009.

H. Jang, A. Robertson, and R. Seth. Transverse dimensions of wood pulp fibres by confocal laser scanning microscopy and image analysis. *Journal of Materials Science*, 27:6391–6400, 1992.

H. F. Jang, R. S. Seth, C. B. Wu, and B. K. Chan. Determining the transverse dimensions of fibers in wood using confocal microscopy. *Wood and Fiber Science*, 37(4):615–628, Oct. 2005.

A. Johansson. Correlations between fibre properties and paper properties. Masters thesis, KTH Royal Institute of Technology, 2011.

P. Kontscheider, M. Donoser, H. Bischof, K. Kritzinger, and W. Bauer. Detecting paper fibre cross sections in microtomy images. *20th Intl. Conf. on Pattern Recognition*, pages 316–319, 2010.

C. Lu, L. Latecki, N. Adluru, X. Yang, and L. Haibin. Shape guided contour grouping with particle filters. *IEEE 12th International Conference on Computer Vision*, pages 2288–2295, 2009.

J. Matas, O. Chum, M. Urban, and T. Pajdla. Robust wide baseline stereo from maximally stable extremal regions. *Image and Vision Computing*, 22:761–767, 2004.

T. L. Mithrush. An experimental study of fluid flow in a low consistency refiner. Masters thesis, The University of British Columbia, Nov. 2013.

N. Otsu. A threshold selection method from gray-level histograms. *IEEE Transactions on Systems, Man, and Cybernetics*, 9(1):62–66, Jan. 1979.

P. Reme, P. Johnsen, and T. Helle. Assesment of fibre transverse dimensions using SEM and image analysis. *Journal of Pulp and Paper Science*, 28(4):122–128, Apr. 2002.

K. Schulgasser and D. Page. The influence of tranverse fibre properties on the in-plane elastic behaviour of paper. *Composites Science and Technology*, 32(4):279 – 292, 1988.

R. Seth. Fibre quality factors in papermaking, the importance of fibre coarseness. *MRS Proceedings*, 197:143, 1990. doi: 10.1557/PROC-197-143.

Y. Sharma, A. B. Phillion, and D. M. Martinez. Automated segmentation of wood fibres in micro-CT images of paper. *Journal of Microscopy*, 260(3):400–410, 2015. ISSN 13652818. doi: 10.1111/jmi.12308.

P. Watson and M. Bradley. Canadian pulp fibre morphology: Superiority and considerations for end use potential. *The Forestry Chronicle*, 85:401–408, 2009.

P. J. Withers. X-ray nanotomography. *Materials Today*, 10(12):26–34, 2007. ISSN 13697021. doi: 10.1016/S1369-7021(07)70305-X.

B. Xu and Y.-L. Ting. Fiber-image analysis part II: Measurement of general geometric properties of fibers. *Journal of the Textile Institute*, 87(2):284–295, 1996.